Checkerboard-ordered pattern of $Bi_{0.5}Sr_{0.5}MnO_3$ low-temperature phase probed by x-ray resonant scattering

G. Subías,[1] J. García,[1,*] P. Beran,[2] M. Nevřiva,[3] M. C. Sánchez,[1] and J. L. García-Muñoz[2]
[1]*Instituto de Ciencia de Materiales de Aragón, Departamento de Física de la Materia Condensada, CSIC-Universidad de Zaragoza, C/Pedro Cerbuna 12, 50009 Zaragoza, Spain*
[2]*Institut de Ciència de Materials de Barcelona, CSIC, Campus Universitari de Bellaterra, E-08193 Bellaterra, Spain*
[3]*Institute of Chemical Technology, Technická 5, 16628 Prague 6, Czech Republic*
(Received 31 May 2005; revised manuscript received 10 April 2006; published 12 May 2006)

Resonant x-ray scattering (RXS) at the Mn *K* edge has been used to characterize the low temperature ordered phase of $Bi_{0.5}Sr_{0.5}MnO_3$. Strong resonances were observed for the (030), (050), (05/20), (0 7/2 0), $(4\ \frac{1}{2}\ 0)$, and $(3\ \frac{1}{2}\ 0)$ reflections as the photon energy is tuned through the Mn *K* edge. The reported azimuthal and polarization dependence of the resonant intensities indicates that the low temperature phase is described as a checkerboard ordering of two types of Mn sites with different local geometrical structures. One of the sites is *anisotropic*, a tetragonal distorted oxygen octahedron and the other one is *isotropic*, a nearly undistorted oxygen octahedron. The distinction of these two Mn sites is accompanied by a displacement of the Mn atoms transverse to the *b* axis. We conclude that this checkerboard-ordered pattern is a common ground state in half-doped manganites. Intermediate valence states according to fractional charge segregation were deduced for the two nonequivalent Mn atoms, far from the localized Mn^{3+} and Mn^{4+} ionic species. Hence, the experimental data discard the ionic model of charge and orbital ordering of localized $3d$ (or $3d$-like) states at the Mn site (or the MnO_6 cluster). We suggest a description of the RXS in terms of band structure effects and lattice dynamics.

DOI: 10.1103/PhysRevB.73.205107 PACS number(s): 75.47.Lx, 61.10.−i, 71.30.+h

I. INTRODUCTION

Charge ordering (CO) into charge stripes has become nowadays an important area of research in transition metal oxides due to its role in cuprate superconductivity[1] or manganite colossal magnetoresistance.[2] Initially, CO in the manganite perovskites was generally understood in a purely ionic picture:[3] viewed as a spatially ordering of Mn^{3+} and Mn^{4+} ions in the lattice. This order is accompanied by orbital order (OO), i.e., an ordered occupation of the e_g orbitals. In many cases, it is associated with a Jahn-Teller distortion of the high spin $3d^4$ Mn^{3+} state. Among the common features of the CO transition in manganites, three key characteristics are the increase in the electrical resistivity, a structural transition to a modulated phase and, at low temperatures, the development of long-range charge-exchange (CE)-type antiferromagnetic (AF) order.

The typical and paradigmatic examples of CO insulators are the half-doped $Ln_{0.5}A_{0.5}MnO_3$ (Ln=La or rare earths and A=Ca,Sr) perovskites. The generally accepted model of ordering[4] is based on the checkerboard arrangement of Jahn-Teller distorted $Mn^{3+}O_6$ and nondistorted $Mn^{4+}O_6$ octahedra [Fig. 1(a)]. In these oxides with an orthorhombic *Pbnm* structure at RT, the CO-OO transition is characterized by the onset of superstructure reflections doubling the *b* axis. In the orthorhombic notation, CO reflections will occur at $(0,k,0)$ and OO reflections at $(0,k/2,0)$ with k odd. Diffraction data on these systems is hardly compatible with a complete Mn^{3+} and Mn^{4+} separation, and fractional charge segregation gives better agreement with diffraction results.[4–6] An alternative model emerges from recent studies[7] of a single crystal of $Pr_{0.6}Ca_{0.4}MnO_3$ (having the same modulation as $x=0.5$), which have proposed the formation of Zener polarons (ZP): the e_g electron is trapped in Mn dimmers instead of in a single Mn ion [Fig. 1(b)]. Hence, all Mn sites allocate the same charge. In this new scenario, the CO phase is under-

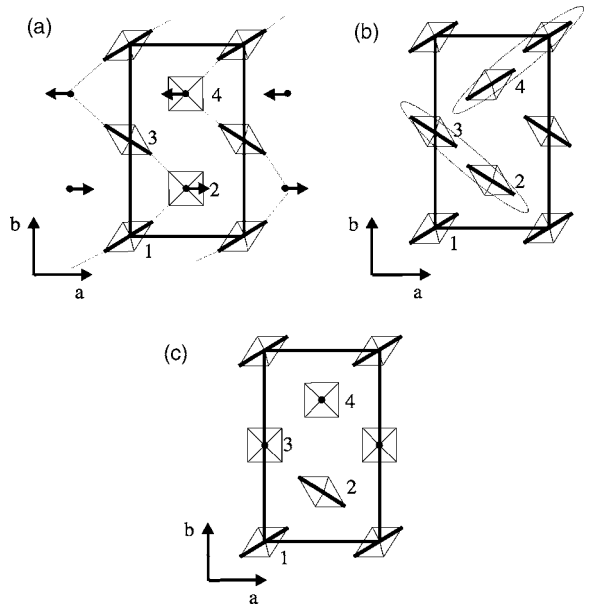

FIG. 1. Schematic diagram of the models of ordering proposed for the low temperature superstructure cell in half-doped manganites: (a) Checkerboard-type model; (b) Zener polaron (ZP) model, and (c) bistriped "2+2" model. The projection shows the *a*-*b* plane. "anisotropic" and "isotropic" Mn atoms are represented by elongated rhombs and squares, respectively, in models (a) and (c). Zener pairs are marked by dashed lobules in model (b). Arrows indicate the displacements of the "isotropic" Mn atoms along the *a* axis and the *zigzag* pattern is marked by dotted lines.

stood as an ordered phase of ZP, this particular ordering giving rise to an AF coupling between *zigzag* chains of ferromagnetic (FM) coupled Zener units. It is difficult to distinguish between these different structural models by x-ray or neutron powder diffraction because of the small number of weak superstructure reflections observable. Nevertheless, recent RXS experiments[8–10] at the Mn *K* edge in several half-doped rare-earth manganites have supported the checkerboard arrangement of two distinct Mn sites with different local oxygen environments though the charge disproportionation is found to be much smaller than 1. It was proposed[8,10] that the so-called CO-OO transition is then a structural phase transition where the two distinct Mn octahedra, one being tetragonal-distorted and the other nearly nondistorted, order in the low temperature phase. The so-called CO reflections [hereafter referring to $(0,k,0)$ reflections, k odd] appear due to the different local structure of these two Mn atoms and the so-called OO reflections [hereafter referring to $(0,k/2,0)$ reflections, k odd] arise from the new translation symmetry generated by the anisotropy induced by the tetragonal distortion.

Bismuth-based manganites ($Bi_{1-x}M_xMnO_3$ M=Ca,Sr) have received great attention due to the observation of some singularities that differ from the general behavior of previously studied manganites. For instance, an extraordinary enhancement of T_{CO} has been reported for these systems. $Bi_{0.5}Ca_{0.5}MnO_3$ displays CO above room temperature[11] ($T_{CO}\approx 325$ K) while the CO-OO temperature in $Bi_{0.5}Sr_{0.5}MnO_3$ is approximately 200 K above the ordering temperature in $Bi_{0.5}Ca_{0.5}MnO_3$ ($T_{CO}=525$ K in $Bi_{0.5}Sr_{0.5}MnO_3$, Refs. 12 and 13). Moreover $Bi_{0.75}Sr_{0.25}MnO_3$ (Ref. 14) undergoes a CO transition at $T_{CO}=600$ K, well above the ordering temperature in half-doped $Bi_{0.5}Sr_{0.5}MnO_3$. The observed structural changes confirm a new type of CO in $Bi_{0.75}Sr_{0.25}MnO_3$, which is very stable against temperature and compositional fluctuations. This spectacular enhancement of the tendency of charges to localize and order has been attributed to the particular electronic structure of the Bi^{3+} ions, having a highly polarizable $6s^2$ lone pair that can hybridize with O $2p$ states. In fact, Bi^{3+} and La^{3+} have an almost similar ionic radii of 1.24 Å and 1.22 Å, respectively for nine-coordination,[15] though $BiMnO_3$ is FM in contrast to the AF (A-type) order of $LaMnO_3$. The magnetization of the $Bi_{1-x}Sr_xMnO_3$ system[16,17] shows that the FM moment decreases with increasing x and only vanishes at $x\approx 0.4$. All these $Bi_{1-x}Sr_xMnO_3$ ($x\leqslant 0.5$) manganites remain semiconductor up to room temperature. A jump in the resistivity is observed associated with the onset of the CO transition, similar to rare earth manganites.[18] However, marked differences are found when comparing the physical properties of low-doped (Bi,Sr)MnO_3 compounds to other known $R_{1-x}A_xMnO_3$ manganites at the same doping level.[19]

To understand the specific behavior of bismuth-based manganites, it is of interest to investigate in detail the low temperature ordered phase in these oxides. High-resolution electron microscopy studies of the $Bi_{1-x}Sr_xMnO_3$ series[13,20] have proposed a distinctive feature for highly stable CO phases in Bi-Sr-Mn-O compounds: a contrast modulation characterized by alternating double rows of MnO_6 octahedra parallel to the Mn layers. Based on these observations, a new type of modulated structure [Fig. 1(c)] was proposed. The model is built up of double Mn^{3+} stripes alternating with double (denoted as 2:2) and quadruple (2:4) Mn^{4+} stripes for $x=1/2$ and $x=2/3$, respectively. This type of CO pattern (hereafter called "bistriped") differs both from the conventional checkerboard pattern where Mn^{3+} and Mn^{4+} single stripes alternate [Fig. 1(a)] and from the ZP model [Fig. 1(b)].

In this paper, we will mainly focus on the description of the low temperature ordered phase of the $Bi_{0.5}Sr_{0.5}MnO_3$ compound. This sample presents the so-called CO transition at temperatures ~525 K. The characteristic lattice deformation evolves with decreasing temperature and saturates above 300 K, CO being fully established at room temperature.[18] An AF ordering of mainly CE-type was detected at low temperatures below $T_N=155$ K.[17] We present a study of the charge modulation in $Bi_{0.5}Sr_{0.5}MnO_3$ at room temperature by RXS experiments at the Mn *K* edge. Detailed measurements of the polarization and azimuthal dependence of $(0,k,0)$ and $(0,k/2,0)$ (k=odd) resonant intensities have been carried out to determine their origin and consequently, to probe the ordering model. The temperature dependence on heating above T_{CO} has also been studied, including the evolution of the intensities, wave vectors, and correlation lengths. Our results show that the ordered phase of $Bi_{0.5}Sr_{0.5}MnO_3$ is perfectly described by a checkerboard arrangement of two distinct Mn atoms because of their different local geometrical structure, as it has been previously proposed for half-doped rare earth manganites.[8,10] Intermediate-valence states were deduced though a small charge disproportionation ($\approx 15\%$) exists. The present experiment also discards both, the bistriped (2:2) and the ZP models.

II. EXPERIMENTAL METHOD

Single crystals of $Bi_{0.5}Sr_{0.5}MnO_3$ have been grown by the conventional flux method, with the excess of Bi_2O_3 used as flux. Stoichiometric ratios of the precursors Bi_2O_3, $SrMnO_3$ and MnO_2 were mixed in agate mortar ($SrMnO_3$ was prepared by standard solid state reaction from $SrCO_3$ and $MnCO_3$ sintered at 800 °C several times on air). Additional Bi_2O_3 was added to the mixture (wt %(flux)=82.5%). The mixture (precursors and flux) was placed into a platinum crucible and preheated at 700 °C for 12 h. The liquid ($T_L=1120$ °C) and the eutectic ($T_E=741$ °C) temperatures were determined. After a preheating period at T_L+50 K (duration 12 h), the growth was started at T_L+5 K by decreasing the temperature at the rate 1 K/h down to the final temperature T_E+50 K, at which the furnace was turned off and the solution cooled down to room temperature. The crystals were separated from flux by heating in a solution of nitric acid. Previous characterization of the crystal included electron diffraction, energy dispersive spectroscopy (EDS), single crystal x-ray and neutron diffraction, synchrotron x-ray powder diffraction, etc. The chemical composition has been verified by Rietveld analysis of diffraction data and by electron microanalysis.[18] The average composition is close to $Bi_{0.48\pm0.04}Sr_{0.51\pm0.04}MnO_3$. At room temperature, the average

structure is well described using an orthorhombic *Ibmm* cell with $a=5.539$ Å, $b=5.530$ Å, and $c=7.587$ Å. The CO superstructure results from the orthorhombic cell doubled along the b axis. A polished $(110)_{\text{cubic}}$ surface in the pseudocubic setting of a twinned sample was used for the RXS study. The twinned crystal has both (100) and (010) oriented domains at the sample surface so that both $(h00)$- and $(0k0)$-type reflections are accessible at nearly the same scattering angle. The mosaic of the sample was 0.25° [full width half maximum (FWHM)] as measured at the (020) reflection. The basic transport and magnetic properties of the single crystal used in the present study have been described in detail elsewhere.[18]

The RXS experiments were performed at the magnetic scattering undulator beamline[21] ID20 at the European Synchrotron Radiation Facility (E.S.R.F., Grenoble). A double-crystal Si(111) monochromator located between two focusing mirrors was used to define the energy band around the Mn K edge with an energy resolution about 1 eV and a high degree of linear σ polarization. We report the energy dependence of the diffracted intensity, as it is tuned through the Mn-K absorption edge (6550.6 eV as defined by the inflection point of the fluorescence spectrum), of the (030), (050), (05/20), (07/20), (41/20), and (31/20) reflections. Azimuthal scans were also performed rotating the sample by an angle ϕ around the diffraction vector $\mathbf{Q}=\mathbf{k}'-\mathbf{k}$. Special care was taken to avoid multiple scattering by slightly changing the value of the azimuthal angle ϕ. The scattered beam was resolved into the respective σ-σ' and σ-π' polarization channels where σ (π) denotes the polarization perpendicular (parallel) to the scattering plane. The polarization analysis was performed using a Cu(220) crystal analyzer for which $2\theta_{\text{Bragg}} \approx 96°$ at the Mn K edge. The discrepancy from the ideal value of 90 degrees leads to a leakage for the projection of one polarization component into the other one. By measuring the fully σ-σ' polarized Bragg reflection (020) in the σ-π' polarization channel, we estimated the leakage to be about 2%. It gives a longitudinal resolution of 0.008 $Å^{-1}$ [half width half maximum (HWHM)].

Figure 2 displays the temperature evolution of the integrated intensities of (030) and (05/20) reflections on resonance at the Mn K edge. Both kinds of reflections disappear on heating at around 480 K, coupled to the decrease of the electrical resistivity (see the inset of Fig. 2). This evolution shows that the characteristic structural modulations occur at the onset of the so-called CO-OO transition. We will discuss the detailed temperature dependence of both types of superstructure reflections later on.

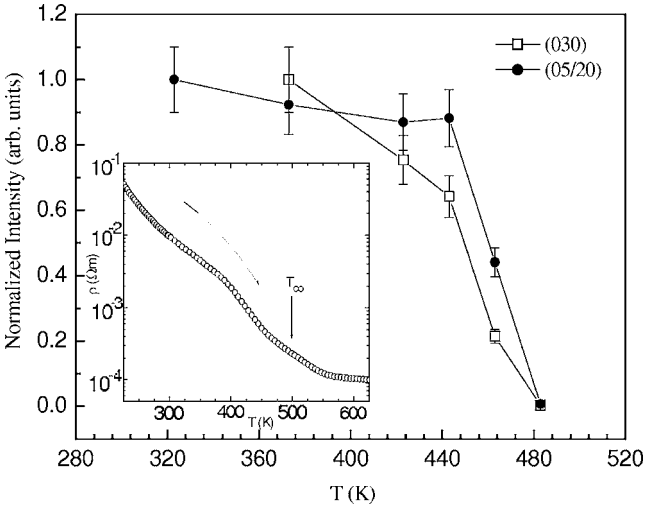

FIG. 2. Integrated intensity of (030) and (05/20) superstructure reflections of the $Bi_{0.5}Sr_{0.5}MnO_3$ single crystal on resonance as a function of temperature, which implies a transition temperature T_{CO}, of 480 K. Integrated intensities have been normalized to 1 at room temperature. Inset: The jump in the electrical resistivity on heating, showing the onset of the CO-OO transition (Ref. 18).

III. EXPERIMENTAL RESULTS

A. $(0,k,0)$ k=odd reflections

Figure 3 shows the evolution of the σ-σ' polarized intensity of both (030) and (050) reflections across the Mn K edge at room temperature at different azimuth angles. A similar line shape versus incident photon energy is observed for both reflections: a nonresonant Thomson scattering at energies below the absorption edge, a broad resonant peak at the Mn K edge, and additional fine structure at energies above the absorption edge. The fact that spectra of the $(0,k,0)$ k odd reflections are independent of the $\mathbf{k}$ wave vector confirms, as expected, the dipole $(1s \rightarrow np)$ character of the resonant scattering.[22] The main resonance is located at 6553 and 6552.3 eV for (030) and (050) reflections, respectively. The slight difference between the two maxima is due to the interference process between the resonant and nonresonant contributions, which depends on the magnitude of the nonresonant intensity.[8] Differences in the intensity and profile of the $(0,k,0)$ resonance for different k values are also explained in terms of the different values of the Thomson scattering. In addition, the existence of this Thomson scattering has been observed before in other halfdoped manganites[8,9] and it has been related to structural modulations coming from small displacements of the atoms out of the *Pbnm* symmetry.

A strong variation of the intensity of the main resonance is also observed as a function of the azimuth angle for both reflections. It shows a minimum for $\phi \sim 0°$ and a maximum for $\phi \sim 90°$, nonvanishing the intensity at the minimum. Moreover, the azimuthal evolution does not affect only the intensity at the resonant peak but a small energy shift together with a slight change in the line shape are also detected from Fig. 3. At $\phi=0°$ and $-10°$, the resonant peaks are located at 6554.3 and 6553.8 eV for (030) and (050) reflections, respectively. The azimuthal evolution of the integrated intensity (θ scan) of these reflections in the σ-σ' geometry at fixed energy, intermediate between the main resonance at $\phi=0°$ and $\phi=90°$, is shown in Fig. 4 for rotations over 180°. The resonant scattering exhibits the same sinusoidal behavior for (030) and (050) reflections with π period in contrast to the nonresonant Thomson scattering (crosses), which is independent of the azimuth angle as expected. This nonresonant contribution is stronger for (030) than for the (050) reflec-

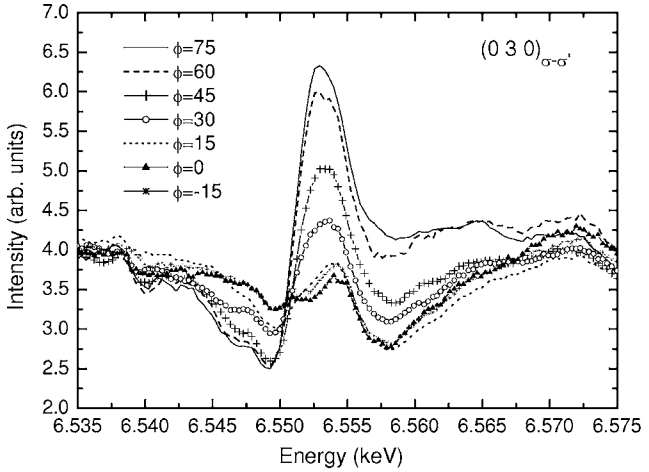

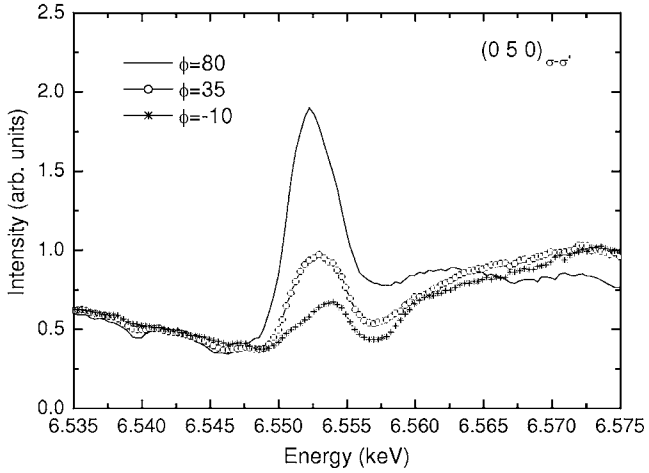

FIG. 3. Energy dependence of the intensity of the $(030)_{\sigma\text{-}\sigma'}$ and $(050)_{\sigma\text{-}\sigma'}$ reflections near the Mn K edge at room temperature at different azimuth angles ϕ. The azimuth angle $\phi=0°$ corresponds to an incident σ polarization along the c axis.

tion. It is noteworthy that the intensity approaches the nonresonant contribution when $\phi\sim 0°$ (minimum) in contrast to the expected azimuthal behavior of a resonant reflection coming purely from CO (the atomic anomalous scattering factor is scalar). For the latter, a constant resonant contribution must be added independent of the azimuth angle. We will discuss this point later on when we develop the structural model for the description of this behavior.

B. $(0,k/2,0)$ k=odd reflections

Figure 5 shows the energy dependence of (0 5/2 0) and (0 7/2 0) reflections across the Mn K edge in the σ-π' channel at $\phi=70°$. A large resonant signal is observed at energies close to the Mn absorption edge (6551.7 eV) for both half-integer reflections, with the same Gaussian line shape independent of the incident and diffracted wave vectors. In addition, a small peak is observed at ~6538 eV in the spectrum of the (0 7/2 0) reflection that corresponds to the prepeak energy in the absorption spectrum. No signal was observed at energies below the absorption edge, implying that only pure resonant scattering is present. As for the $(0,k,0)$ k odd reflections, this resonant scattering involves dipole $1s\rightarrow np$ transitions. Polarization analysis indicates that the scattered intensity is predominantly π polarized as it is shown in the inset of Fig. 5. Energy dependence of the (0 5/2 0) reflection at selected azimuth angles is reported in Fig. 6. No new features are introduced varying the azimuth angle except for a variation of the overall intensity. As a function of the azimuth angle (see the inset of Fig. 6), integrated intensities for both (0 5/2 0) and (0 7/2 0) reflections take a maximum intensity at $\phi\approx 90°$, disappearing completely around $\phi\approx 0°$.

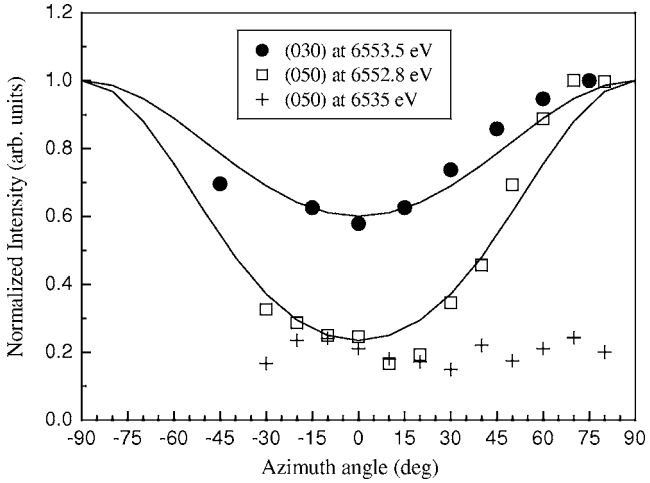

FIG. 4. Azimuthal dependence of the $(030)_{\sigma\text{-}\sigma'}$ and $(050)_{\sigma\text{-}\sigma'}$ integrated intensities at fixed energies, (1) 6535 eV well below the Mn K edge resonance and (2) 6553.5 and 6552.8 eV around the maximum of the Mn K edge resonances at (030) and (050) reflections, respectively. Integrated intensities have been normalized by the value at $\phi\sim 75°$, near the maximum, for the sake of comparison. Solid lines are the best-fit curves from the structural checkerboard model.

We note that all these results, including the energy line shape, the polarization and azimuthal dependence, and the

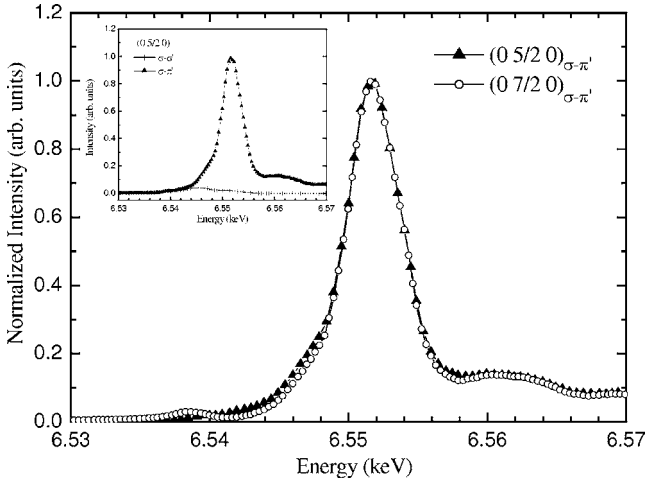

FIG. 5. Intensity plotted versus incident photon energy through the Mn K edge of the $(05/20)_{\sigma\text{-}\pi'}$ and $(07/20)_{\sigma\text{-}\pi'}$ reflections at room temperature ($T<T_{CO}$). Intensity has been normalized at the maximum of the resonance for comparison. Inset: Comparison of the energy dependence of the (05/20) measured in the two σ-σ' and σ-π' scattering channels at $\phi=70°$.

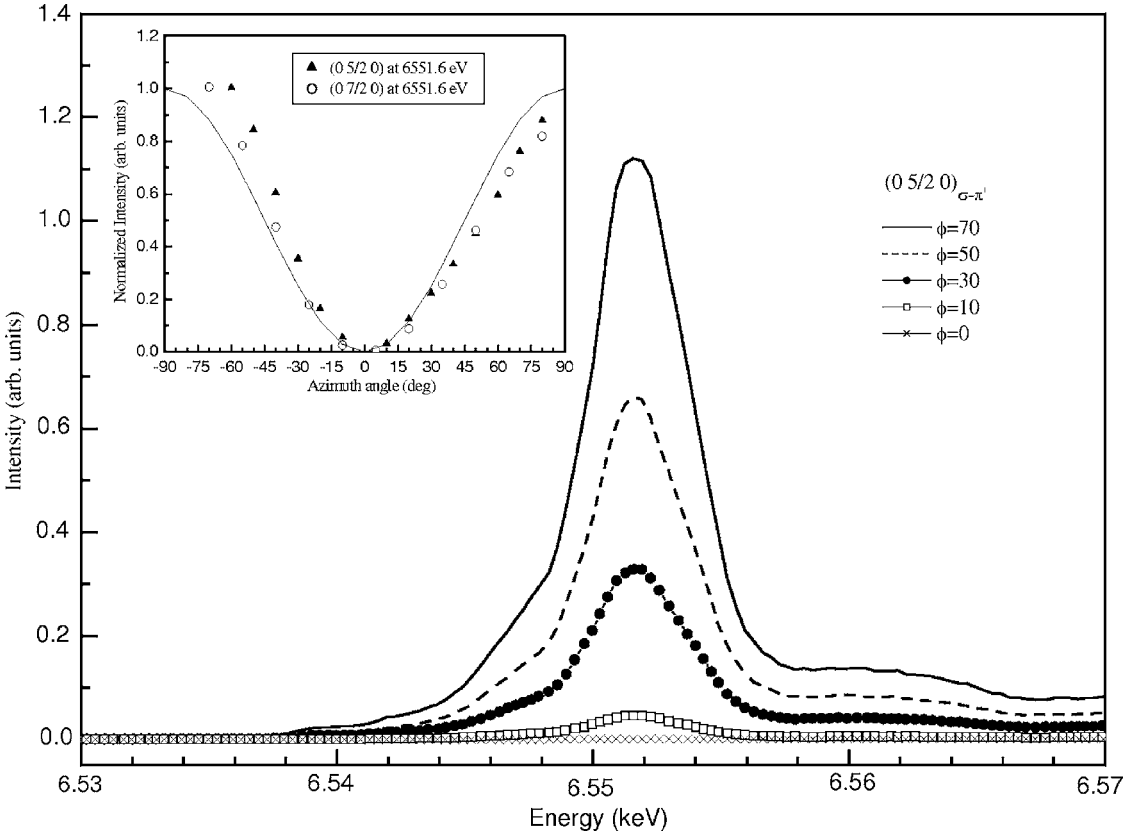

FIG. 6. Energy dependence of the intensity of the $(05/20)\sigma$-π' reflection near the Mn K edge at room temperature at different azimuth angles ϕ. The azimuth angle $\phi=0°$ corresponds to an incident σ polarization along the c axis. Inset: Azimuthal dependence of the $(05/20)_{\sigma\text{-}\pi'}$ and $(07/20)_{\sigma\text{-}\pi'}$ integrated intensities at the maximum of the Mn K edge resonance. Integrated intensities have been normalized by the value at $\phi\sim-70°$, near the maximum, for the sake of comparison. Solid lines are the best-fit curves from the structural checkerboard model.

absence of nonresonant scattering away from the absorption edge, are similar to those reported previously at half-integer reflections of $Pr_{0.6}Ca_{0.4}MnO_3$ (Ref. 9) and $Nd_{0.5}Sr_{0.5}MnO_3$ (Ref. 10). This similarity is a strong indication that the origin of these half-integer reflections—the anisotropy of the Mn anomalous scattering factor—is the same in all these materials.

C. $(h,k/2,0)$ $h\neq 0$ and k=odd reflections

We have also performed scans of $(4\ \frac{1}{2}\ 0)$ and $(3\ \frac{1}{2}\ 0)$ reflections in both σ-σ' and σ-π' scattering channels. Figure 7 reports the polarized-resolved energy dependence for both reflections at $\phi=75°$, i.e., the value for which the maximum resonant intensity of $(0k0)$ and $(0k/20)$ k=odd reflections was detected. The σ-π' scattering of the $(h\ \frac{1}{2}\ 0)$ reflections shows a strong resonance at the Mn K edge similar to the one observed for the $(0k/20)$ k=odd reflections (Fig. 7, lower panel). In contrast, a significant σ-σ' scattering is only observed for $(h\ \frac{1}{2}\ 0)$ reflections with $h\neq 0$, exhibiting a pronounced deep at the absorption edge and a fine structure at energies above the edge (Fig. 7, upper panel). This cusp drop in the diffracted intensity is characteristic for the energy dependence through the Mn K edge of a Bragg reflection due to the interference effect between the Thomson scattering term and the real part of the anomalous scattering term.[23] The observation of σ-σ' intensity for both, $(4\ \frac{1}{2}\ 0)$ and $(3\ \frac{1}{2}\ 0)$ reflections, together with the extinction of this σ-σ' scattering channel for $(0k/20)$ k=odd reflections implies a lattice modulation transversal to the b axis that it must involve displacements of the Mn atoms as well as possibly Bi/Sr and O ones. We note here that the apparent nonresonant σ-π' scattering of the $(h\ \frac{1}{2}\ 0)$ reflections at energies below the edge agrees well with the leakage from the σ-σ' channel of the present crystal analyzer. For completeness the energy dependence of both $(4\ \frac{1}{2}\ 0)_{\sigma\text{-}\pi'}$ and $(3\ \frac{1}{2}\ 0)_{\sigma\text{-}\pi'}$ reflections at $\phi=0°$, correspondent to the minimum in the resonant intensity of $(0k0)$ and $(0k/20)$ k=odd reflections, is also reported in the lower panel of Fig. 7 (solid lines). The large resonant peak observed at $\phi=75°$ has completely disappeared and a 2% leakage from the σ-σ' channel of the analyzer is sufficient to account for the remaining intensity.

This type of superstructure reflections has been already identified in $Bi_{0.5}Sr_{0.5}MnO_3$ from synchrotron x-ray powder diffraction data.[12] Moreover, such modulations have also been observed in other half-doped manganites with CE-type structures and in particular, in $La_{0.5}Ca_{0.5}MnO_3$ (Ref. 4). We will show that the azimuthal and polarization dependence of these $(h\ k/2\ 0)$ k=odd reflections in $Bi_{0.5}Sr_{0.5}MnO_3$ can be described by considering a model with the nondistorted Mn

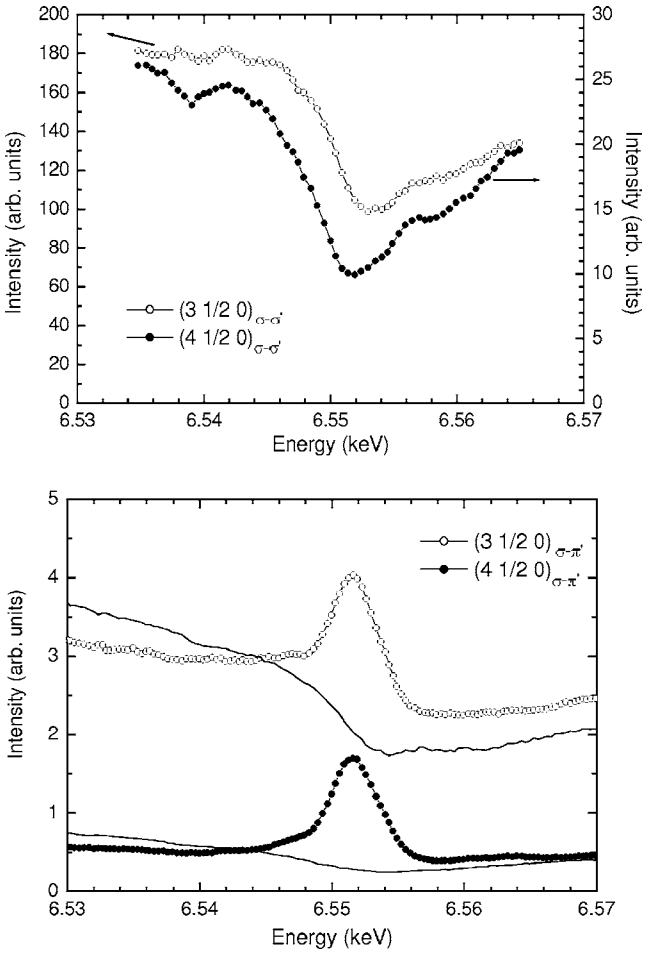

FIG. 7. Polarization-resolved energy scans of (3 1/2 0) (line +open circles) and (4 1/2 0) (line+closed circles) reflections at $\phi = 75°$ in the σ-σ' (upper panel) and σ-π' (lower panel) scattering channels. The energy dependence of the σ-π' scattered intensity at $\phi = 0°$ (solid lines) for both reflections is also shown for comparison.

atoms of the checkerboard structure displaced along the [100] direction (transverse modulation).

D. Temperature dependence

The temperature evolution of the energy scans of the (030) (σ-σ' scattering) and (05/20) (σ-π' scattering) reflections between 373 and 483 K is shown in Fig. 8. First, the energy line shape of both reflections remains nearly alike in the whole temperature range. On the other hand, the intensities slightly decrease from 373 K up to about 440 K but drop abruptly between 440 and 480 K, near T_{CO}, reaching almost zero. It is also clear from Fig. 8 that the temperature dependences of the resonant and nonresonant intensities for the (030) reflection are identical. This suggests that the lattice modulation accompanying the superstructure (0k0) peaks reflects the same order parameter. As shown in Fig. 2, the fact that the two (0k0) and (0k/20) reflections disappear nearly at the same temperature suggests that both superstructure orderings might be coupled although small differences in their respective thermal evolutions are observed.

θ-2θ scans of each reflection as a function of temperature are also shown as insets of Fig. 8, off from resonance ($E = 6535$ eV) for (030) and on the resonance ($E = 6551.7$ eV) for (05/20). The (030) reflection remains commensurate with the lattice throughout the ordered phase, independent of temperature. On the other hand, a small change from $k = 2.5$ down to $k = 2.465$ reciprocal lattice units was found for the (05/20) reflection between 463 and 483 K, just at the phase transition, remaining nearly commensurate in the whole temperature range below the transition. Furthermore, the width shows an increase just at the transition where the signal has almost disappeared. These results are in agreement with the results of other RXS experiments previously reported for $Pr_{0.6}Ca_{0.4}MnO_3$ (Ref. 24) or $Nd_{0.5}Sr_{0.5}MnO_3$ (Ref. 10), which do not report any signature of incommensurability throughout the ordering phase. However, a lack of consensus on the commensurability/incommensurability of the CO/OO ordering in half-doped manganites still exists.[25] Finally, θ-scans of the Bragg (020) reflection and the so-called CO (030) and OO (05/20) reflections at room temperature are compared in Fig. 9. It is clear from the figure that the three peaks have similar widths, implying that the correlation lengths of (0k0) and (0k/20) with k odd reflections are the same as that of the structure.

IV. ANALYSIS

We have reported a strong resonant effect at the superstructure reflections $(05/20)_{\sigma\text{-}\pi'}$, $(030)_{\sigma\text{-}\sigma'}$, $(07/20)_{\sigma\text{-}\pi'}$, $(050)_{\sigma\text{-}\sigma'}$, $\left(3\frac{1}{2}0\right)_{\sigma\text{-}\pi'}$ and $\left(4\frac{1}{2}0\right)_{\sigma\text{-}\pi'}$ near the Mn K edge at room temperature ($T < T_{CO}$) in a $Bi_{0.5}Sr_{0.5}MnO_3$ single crystal. These two sets of peaks, (i) $\mathbf{Q}+(010)$ and (ii) $\mathbf{Q}+(01/20)$ with $\mathbf{Q}$ the diffraction vector of the Bragg reflections in the *Ibmm* structure, had been already observed in the low temperature ordered phase of rare earth half-doped manganites,[9,10] showing the same energy, azimuthal, and polarization dependence. For rare earth half-doped manganites, the experimental results supported the checkerboard pattern of essentially two kinds of Mn octahedra: tetragonal distorted (Jahn-Teller-like) and almost nondistorted ones. For $Bi_{0.5}Sr_{0.5}MnO_3$, other ordering models have been proposed, such as the bistriped model[13,20] to account for the unusual high transition temperature or the ZP-model,[7] which proposes FM dimmers in the paramagnetic regime below T_{CO} to explain the discontinuity in the paramagnetic behavior at the transition temperature.

In the following we discuss the experimental results within the framework of the various proposed models: (A) structural checkerboard model, (B) ZP model, and (C) bistriped model. We start from evaluating the expression of the structure factors from the symmetry of the crystal lattice. Below T_{CO}, the superstructure cell doubled along the b axis and it is defined as $a \times 2b \times c$ with 8 Mn atoms (see Fig. 1). As the a-b planes are equivalent along the c axis, it leaves four independent Mn atoms denoted as 1, 2, 3, and 4 in the schematics of Fig. 1. We note here that throughout the paper all crystallographic notations will refer to the *Ibmm* simple crystallographic unit cell. Due to the structural transition at

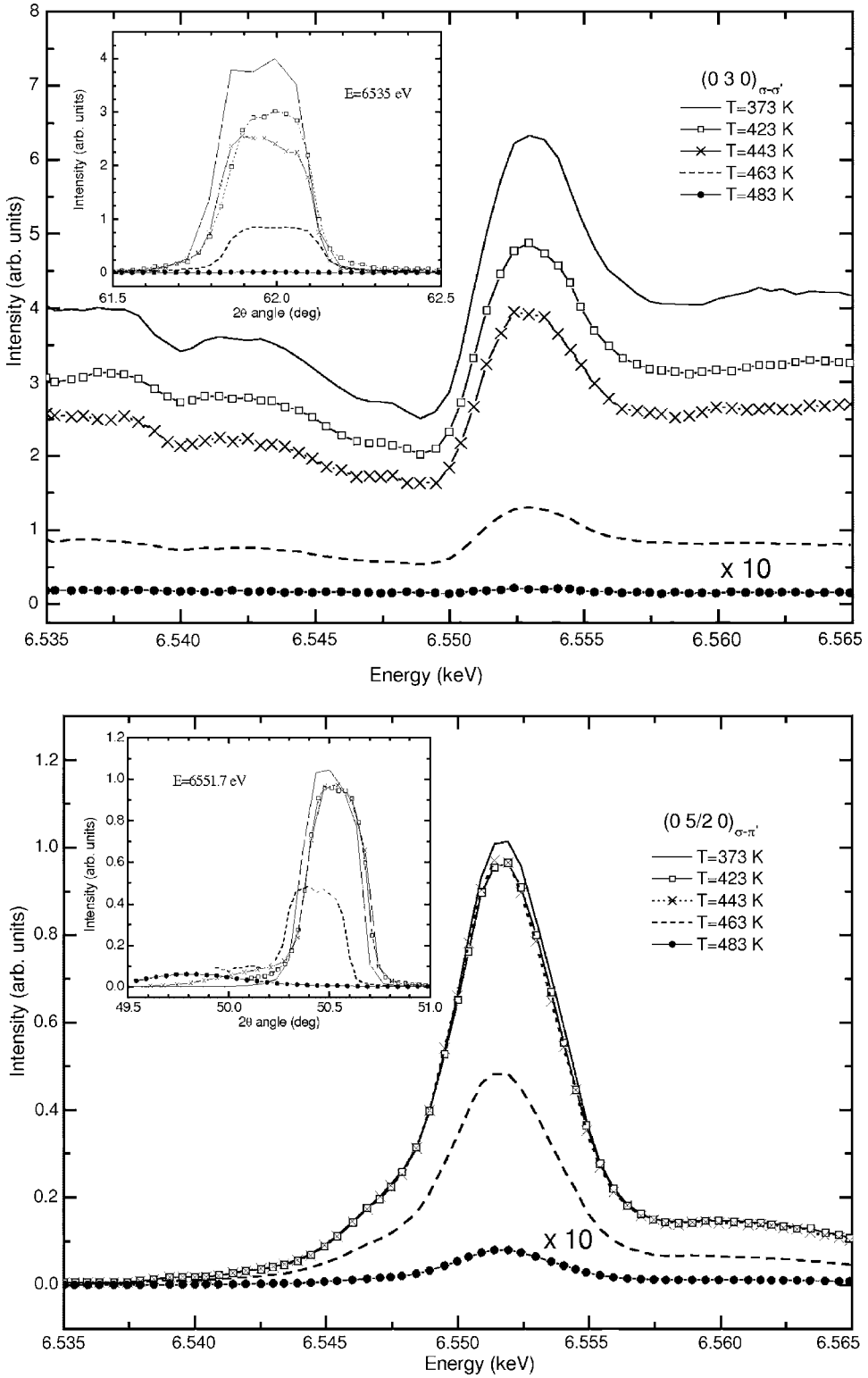

FIG. 8. Temperature dependence of the intensity versus photon energy of the $(030)_{\sigma\text{-}\sigma'}$ (upper panel) and $(05/20)_{\sigma\text{-}\pi'}$ (lower panel) reflections crossing T_{CO} at ϕ maximum. Insets: θ-2θ scans as a function of temperature of the (030) (upper panel) and (05/20) (lower panel) reflections, off-resonance (E=6535 eV) and on-resonance (E=6551.7 eV), respectively.

T_{CO}, the $(0k0)$ (k=odd) reflections are no longer forbidden in the low temperature phase. If we neglect slight displacements of the Mn atoms as a first approximation, the structure factors of $(0k0)$ and $(0k/20)$ reflections with k being odd are:

$$F(0k0) = F(h00) = (f_1 + f_3) - (f_2 + f_4) + C_k(C_h),$$

$$F(0k/20) = f_1 - f_3 \pm i(f_2 - f_4). \quad (1)$$

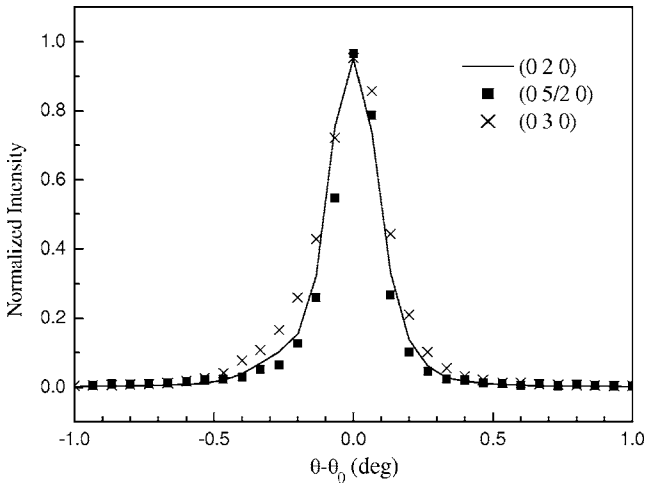

FIG. 9. Longitudinal scans of the Bragg (020) and the so-called CO (030) and OO (05/20) superstructure reflections at room temperature. Data have been normalized to the same peak intensity for comparison purposes.

Here, C_k and C_h take into account the Thomson scattering due to the new crystal symmetry, which also involves nonresonant contributions of the O and/or Bi/Sr atoms after their displacements from the equilibrium positions (C_k and C_h are zero above T_{CO}) and f_i, $i=1,2,3,4$ are the anomalous atomic scattering factors of the 4 Mn sites. We next need to derive the expression for the anomalous atomic scattering factors. The anomalous x-ray scattering process[22] near the Mn *K* edge involves the same physical process as the x-ray absorption spectroscopy so it is dominated by the virtual excitation of a core electron from the Mn 1*s* level to unoccupied *np* states (dipolar *E*1 transition). Since the excited electron strongly interacts with the neighboring atoms, it is sensitive to any anisotropy of the environment and the anomalous scattering factor of the Mn atoms is then anisotropic with a symmetry determined by the local symmetry at the Mn sites.[26] The scattering amplitude is then described as a tensor of rank two within the dipolar approximation (*E*1). Let us now determine the anomalous atomic scattering tensors for the four Mn sites according to each of the three ordering models and, using Eq. (1), the structure factors of the resonant reflections.

A. Structural checkerboard model

The simplest checkerboard model[8,10] for half-doped manganites is based on the crystallographic refinement of Radaelli *et al.*[4] for $La_{0.5}Ca_{0.5}MnO_3$ and consists of a 1:1 ordering of two nonequivalent Mn atoms (forming alternating lines along the *a* or *b* axes), one being *anisotropic* and the other one being *isotropic*. In our description, the anisotropic Mn_1 and Mn_3 octahedra are identical and tetragonal distorted and the isotropic Mn_2 and Mn_4 octahedra are also identical but nearly nondistorted. The tetragonal axis (anisotropy axis) of Mn_1 and Mn_3 is assumed to form 45° between *x* and *y* crystallographic axes as a first approximation so an orientational ordering of the anisotropy axis to form *zigzag* chains along the *b* axis is also proposed within this description [Fig. 1(a)]. At this point, the atomic scattering tensors f_2 and f_4 are diagonal with $f_{xx}=f_{yy}=f_{zz}=f$ and the off-diagonal terms zero. For the sites 1 and 3, $f_\parallel$ and $f_\perp$ are the components along the direction parallel and perpendicular to the tetragonal axis and the atomic scattering tensors f_1 and f_3 in the (x,y,z) coordinate system are expressed in terms of $f_{xx}=f_{yy}=(f_\parallel+f_\perp)/2$; $f_{zz}=f_\perp$; f_{xy} $(Mn_1)=-f_{xy}$ $(Mn_3)=(f_\perp-f_\parallel)/2$ and $f_{xz}=f_{yz}=0$.

The resulting polarization and azimuthal dependence of the resonant scattering of the $(0k0)$ and $(0k/20)$ reflections in this model is expressed as follows (Refs. 8 and 10):

$$I_{\sigma-\sigma'}(h00)=I_{\sigma-\sigma'}(0k0)=[C_h(C_k)+2(f_\perp-f)\cos^2\phi + (f_\parallel+f_\perp-2f)\sin^2\phi]^2,$$

$$I_{\sigma-\pi'}(h00)=I_{\sigma-\pi'}(0k0)=[(f_\perp-f_\parallel)\sin\phi\cos\phi\sin\theta]^2,$$

$$I_{\sigma-\sigma'}(0k/20)=0,$$

$$I_{\sigma-\pi'}(0k/20)=[(f_\parallel-f_\perp)\sin\phi\cos\theta]^2. \quad (2)$$

At the $\mathbf{Q}+(01/20)$ reflections, the Mn_2 and Mn_4 contributions cancel as these atoms are considered as isotropic and the resonant signal comes from the anisotropy of both, Mn_1 and Mn_3 atoms, associated with their identical tetragonal distortion but occurring with different orientation for the two atoms [see Eqs. (1) and (2)]. The observation of a resonance for the $\mathbf{Q}+(010)$ reflections implies that Mn_1-type and Mn_2-type crystallographic sites show a different anisotropy [Eq. (1)] that in our case it is induced by the different local geometry between $Mn_1(Mn_3)$ tetragonal distorted and $Mn_2(Mn_4)$ nondistorted octahedra.

B. Zener polaron model

The refined structure proposed by Daoud-Aladine *et al.*,[7] the so-called ZP model, also presents two nonequivalent Mn sites, both MnO_6 octahedra being slightly elongated and having off-centered Mn atoms [see Fig. 1(b)]. Hence, instead of the distortion pattern described for the checkerboard model, this structure presents all MnO_6 octahedra similarly tetragonal distorted. Moreover, the very similar average Mn-O distance of the two Mn sites [$\sim$1.960 and $\sim$1.955 Å, respectively (Ref. 7)] also agrees with an intermediate valence state for the Mn atoms. In this ZP model, $Mn_{1,4}$ and $Mn_{2,3}$ occupy the two nonequivalent sites, respectively. Consequently, $f_1=f_4$ and $f_2=f_3$ with

$$f_1=\begin{pmatrix} \frac{f_\perp+f_\parallel}{2} & \frac{f_\perp-f_\parallel}{2} & 0 \\ \frac{f_\perp-f_\parallel}{2} & \frac{f_\perp+f_\parallel}{2} & 0 \\ 0 & 0 & f_\perp \end{pmatrix}$$

and

$$f_2 = \begin{pmatrix} \frac{f_\perp + f_\parallel}{2} & \frac{f_\parallel - f_\perp}{2} & 0 \\ \frac{f_\parallel - f_\perp}{2} & \frac{f_\perp + f_\parallel}{2} & 0 \\ 0 & 0 & f_\perp \end{pmatrix}. \quad (3)$$

Using Eq. (1), the model gives $I_{\sigma\text{-}\sigma'}(h00) = I_{\sigma\text{-}\sigma'}(0k0) = C_h^2(C_k^2)$, i.e., no resonant contribution at any azimuthal orientation. We would like to mark that even considering displacement of the Mn atoms along the *a* axis, the two "odd" reflections are not resonant in the σ-σ' channel. The empirical observation of a strong resonant effect for $(0k0)$ (k=odd) reflections does not give support to the ZP picture to describe the ordered phase in $Bi_{0.5}Sr_{0.5}MnO_3$. Moreover, the inadequacy of the ZP model to explain the resonant effects observed experimentally at the Mn *K* edge also applies to rare earth half-doped manganites.[9,10]

C. Bistriped model

Finally, the bistriped pattern (proposed by Hervieu *et al.*[13,20]) involves the regular alternation along the *b* axis of two sets of double rows, each set related to a distinct type of MnO_6 octahedra. A model which consists of double stripes of tetragonal-distorted octahedra alternating with double stripes of nondistorted octahedra has been suggested, as shown in Fig. 1(c), based on the existence of the same two kinds of MnO_6 octahedra determined in the checkerboard model (single stripe). Within this type of ordering, Mn_1 and Mn_2 are the anisotropic atoms and Mn_3 and Mn_4 are the isotropic ones so f_1 and f_2 are given by Eq. (3) as for the ZP model and $f_3 = f_4$ is a diagonal tensor with the diagonal terms equal to f. The structure factors for the $(0k0)$ and $(0k/20)$ reflections with k odd in this model are derived from Eq. (1):

$$F(0k0) = F(h00) = f_1 - f_2 + C_k(C_h),$$

$$F(0k/20) = (f_1 \pm if_2) - (1 \pm i)f, \quad (4)$$

and the opposite behavior to the checkerboard model should occur for the intensity of these reflections. In fact, we would observe resonant intensity for the $(0k0)$ reflections only in the σ-π' channel with an energy dependence of the form $[(f_\parallel - f_\perp)\sin\phi]^2$ whereas $I_{\sigma\text{-}\sigma'}$ for the $(0k/20)$ reflections would be proportional to $[2(f_\perp - f)\cos^2\phi + (f_\parallel + f_\perp - 2f)\sin^2\phi]^2$. Again, the observed experimental results are inconsistent with this bistriped model. This kind of arrangement of the Mn atoms in the plane has also been checked for the bilayered $LaSr_2Mn_2O_7$ perovskite,[27] but it was inconsistent with the experimental results in contrast to the checkerboard model.

V. DISCUSSION

Our results show that the checkerboard pattern is the one that satisfactory explains the large resonant effects observed experimentally in the low temperature ordered phases of half-doped $A_{0.5}B_{0.5}MnO_3$ perovskites, independently of the nature of the A and B cations. In order to show that the physical origin of the RXS signal in $Bi_{0.5}Sr_{0.5}MnO_3$ is mainly structural and it does not involve ionic CO and/or OO ordering of localized 3D (or 3D-like) states at the Mn site or the MnO_6 cluster, we analyze the RXS spectrum of the several resonant reflections using a phenomenological description. The checkerboard model used in our data analysis is based on the fact that the anisotropy in the Mn $4p$ band, probed by dipolar $1s$-np transitions at the Mn *K* edge, mainly comes from distortions of the oxygen octahedra surrounding the Mn atoms.[28] The tensors used to describe the anomalous scattering amplitude assume two possible types of distortion: apically elongated and nondistorted MnO_6 octahedra.

Resonant effects mainly occur at the absorption edge. The energy position of the absorption edge is sensitive to both, the charge density on an atom and the anisotropy of the local geometry.[29] In our case, we will define an anisotropic shift (δ_{anis}), which reflects the shift of the energy edge position between the absorption coefficient measured with the polarization vector perpendicular and parallel to the direction of anisotropy (tetragonal axis) for the apically elongated MnO_6, and a chemical shift (δ_{chem}) between the average absorption coefficient of the isotropic (nondistorted) and anisotropic (apically elongated) Mn atoms that can be related to a different charge density. The energy dependence of the anomalous scattering factor is generally described by $f[E] = f'(E) + if''(E)$. The imaginary part is proportional to the absorption coefficient through the optical theorem.[30] The real parts f' are calculated through the Kramers-Kronig transformation of f'', in which Cromer and Liberman's calculation was applied to estimate the region outside the absorption measurements.[31] We have obtained the respective imaginary f'' components from the experimental room temperature XANES spectrum of the $Bi_{0.5}Sr_{0.5}MnO_3$ single crystal measured by fluorescence detection. As resonant peaks appear at the absorption edge, we consider that the main difference between the tensor components of the anomalous scattering factors comes from the different energy position of their absorption edges. In such a way, the energy dependence of the different $f''(E)$ components have been considered as identical to the average XANES spectrum. Then, f'' and f''_{anis} resulted from shifting the average XANES spectrum by $\pm\delta_{chem}/2$, respectively, being f and f_{anis} the average anomalous scattering factor of the isotropic and anisotropic Mn atoms. An energy shift of δ_{anis} was applied between $f''_\parallel$ and $f''_\perp$, where $1/3(f_\parallel + 2f_\perp)$ is defined as the average anomalous scattering factor f_{anis}. Figure 10 shows the real (f') and the imaginary (f'') parts of the different tensor components $f_\parallel$, $f_\perp$ and f obtained by the above procedure on the basis of the chemical (δ_{chem}) and anisotropic (δ_{anis}) rigid energy shifts.

Making use of f' and f'', we modeled the energy dependence of the resonant intensity of the (05/20) and the (030)-(050) reflections at different azimuth angles using as parameters: δ_{anis}, δ_{chem}, and the Thomson scattering factors C_{030} and C_{050}. We estimated Thomson scattering intensities for (030) and (050) reflections from the nonresonant intensity of the Bragg-allowed reflection (020) at 6535 eV given by the crystallographic structure after scaling by their experimental intensity ratios of 3×10^{-4} and 5×10^{-5}, respectively. The results measured intensities reported in Fig. 3 roughly corre-

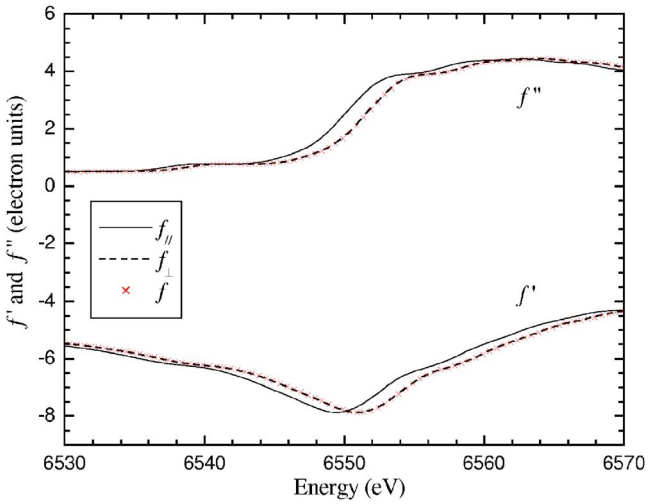

FIG. 10. (Color online) Real f' and imaginary f'' parts of the different tensor components: f (crosses) for the isotropic $Mn_2(Mn_4)$ atoms and $f_{\parallel}$ (solid line) and $f_{\perp}$ (dashed line) for the anisotropic $Mn_1(Mn_3)$ atoms. The anisotropic and chemical energy shifts are defined as $\delta_{anis}=f_{\perp}-f_{\parallel}$ and $\delta_{chem}=\delta+\delta_{anis}/3$ being $\delta=f-f_{\perp}$. Note: $f''(E)\propto E\mu(E)$ were used.

sponded to these estimations. Thus, the Thomson scattering factors resulted in $C_{030}=1.88\pm0.05$ and $C_{050}=0.76\pm0.05$. Following Eq. (2), the absence of resonance in the σ-σ' intensity of $(0k0)$ reflections at $\phi=0°$ would imply f to be equal to $f_{\perp}$. We derived an energy shift δ of 0.1 eV between the isotropic scattering factor f and the perpendicular component $f_{\perp}$ of the anisotropic one from the minimum value of the $(0k0)_{\sigma\text{-}\sigma'}$ resonances at $\phi\sim0°$. The maximum resonant intensity of both, $(0k/20)_{\sigma\text{-}\pi'}$ and $(0k0)_{\sigma\text{-}\sigma'}$ types of reflections is then simulated in terms of δ_{anis} by fixing the value of C_{0k0} and δ. The resulted anisotropic shift δ_{anis} was 1.5 ± 0.2 eV. Finally, the chemical shift was determined as $\delta_{chem}=\delta_{anis}/3+\delta$, i.e., 0.6 ± 0.1 eV.

In Fig. 11, we compare the RXS spectrum drawn from the best-fit simulation with the experimental data for the

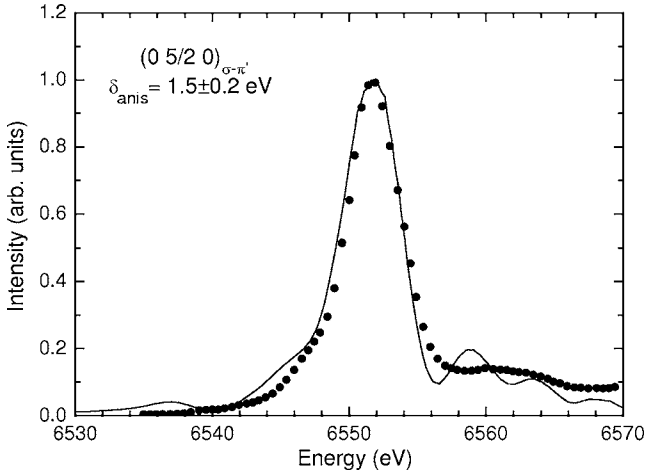

FIG. 11. Best-fit simulation of the $(05/20)_{\sigma\text{-}\pi'}$ spectra (solid line) within the structural checkerboard model [Eq. (2)] compared with the experimental data at $\phi=70°$ (closed circles).

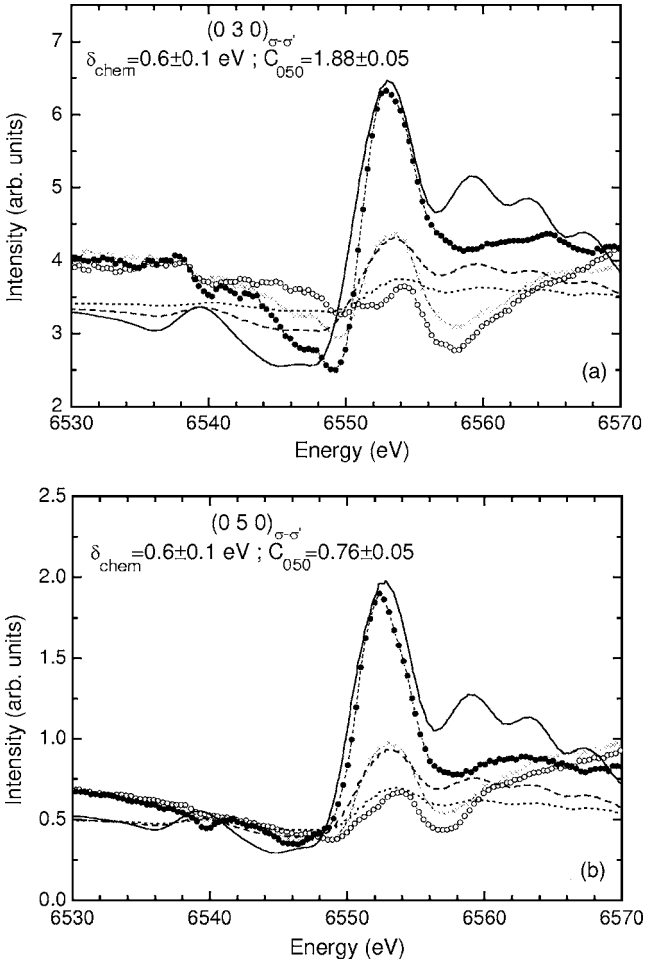

FIG. 12. (a) Best-fit simulations of the $(030)_{\sigma\text{-}\sigma'}$ spectra within the structural checkerboard model [Eq. (2)] at $\phi=75°$ (solid line), $\phi=30°$ (dashed line) and $\phi=0°$ (dotted line) compared with the experimental data ($\phi=75°$-closed circles; $\phi=30°$-crosses and $\phi=0°$-open circles). (b) Best-fit simulations of the $(050)_{\sigma\text{-}\sigma'}$ spectra within the structural checkerboard model [Eq. (2)] at $\phi=80°$ (solid line), $\phi=35°$ (dashed line) and $\phi=-10°$ (dotted line) compared with the experimental data ($\phi=80°$-closed circles; $\phi=35°$-crosses and $\phi=-10°$-open circles).

$(05/20)_{\sigma\text{-}\pi'}$ at $\phi=80°$, near the maximum intensity. Best-fit simulated RXS spectra for the $(030)_{\sigma\text{-}\sigma'}$ and $(050)_{\sigma\text{-}\sigma'}$ reflections are shown in comparison with the experimental data in Fig. 12 at three ϕ values corresponding to maximum, intermediate, and minimum intensities of the azimuthal evolution. This phenomenological model captures qualitative features of the energy dependence of the intensity for the different reflections at various azimuthal angles, which makes the results reliable. Differences are found in the spectral line shape below or just above the resonance that they can be in part due to the approximation that the different tensor components f, $f_{\parallel}$, and $f_{\perp}$ are identical except for a rigid energy shift. However, it reproduces rather well the small differences in the energy position, width, and intensity of the several resonances, which depend on the C value. This model also reproduces the azimuthal dependence of the resonant intensity for the three reflections, as it is shown in Figs. 5 and 7. The solid lines are the fits as given by Eq. (2) with the

maximum resonant intensity normalized to 1.

Finally, the observation of significant σ-σ' nonresonant scattering at $(3\ \frac{1}{2}\ 0)$ and $(4\ \frac{1}{2}\ 0)$ reflections (Fig. 7), which was not observed for $(0\ k/2\ 0)$ reflections requires a displacement of the Mn atoms transversal to the b axis. The simplest model that we can propose for this transverse modulation according to the experimental results consists of a displacement of only the isotropic Mn atoms (denoted as 2 and 4), the same amount Δx along the a axis but in the opposite sense, as represented in Fig. 1(a), whereas the anisotropic Mn atoms (denoted as 1 and 3) are left undisturbed. The resonant scattered intensity in both, σ-σ' and σ-π' channels, is then expressed by

$$I_{\sigma-\sigma'}(hk/20) = [C + 4\pi h \Delta x f]^2,$$

$$I_{\sigma-\pi'}(hk/20) = [(f_{\parallel} - f_{\perp})\sin\phi\cos\theta]^2, \qquad (3')$$

where Δx is the displacement from the atomic x position expressed in fractional coordinates. The variation of the scattered intensity in the σ-σ' channel reported in Fig. 7 (without an absorption correction) is qualitatively consistent with the energy-dependent nonresonant profile of the $(C+af)^2$ term, f being the anomalous scattering factor of the isotropic Mn atoms and C the Thomson scattering.

Summarizing, the proposed phenomenological model in which the shift in the absorption edge energy of the different components of the scattering factors is the main contribution to the appearance of resonances at the Mn K edge correctly describes the polarization and azimuthal dependence of the RXS spectra for the different studied reflections. This result guarantees the validity of the approach used.

The anisotropic energy splitting δ_{anis} is related to the magnitude of the tetragonal distortion of the MnO_6 octahedra. For instance, the XANES calculation[32] of the absorption components of the $1s$ to np dipole transition of the Mn atom in $LaMnO_3$ ($Mn\text{-}O_{long}=2.14$ Å, $Mn\text{-}O_{short}=1.94$ Å) shows a splitting of about 2 eV. Comparing the $(05/20)_{\sigma\text{-}\pi'}$ RXS spectrum of $Bi_{0.5}Sr_{0.5}MnO_3$ ($\delta_{\text{anis}}=1.5\pm0.2$ eV) with that of $Nd_{0.5}Sr_{0.5}MnO_3$ (Ref. 10), where the obtained energy shift δ_{anis} is 1.6 ± 0.2 eV, it is clear that the octahedral tetragonal distortion of the anisotropic Mn atom is similar in the two compounds. This is consistent with the same doping ratio, which implies similar local distortions of the MnO_6 cluster. Concerning δ_{chem}, it is noteworthy that the term *chemical shift* usually denotes an energy shift of the absorption K edge due to different valence states. The obtained δ_{chem} is 0.6 ± 0.1 eV whereas the chemical shift between formal Mn^{3+} and Mn^{4+} oxides[33] reported experimentally is about 4.3 ± 0.2 eV. Following an approximation of a linear correlation of the chemical shift with the charge density on an atom, the charge segregation between the isotropic and the anisotropic Mn atoms in $Bi_{0.5}Sr_{0.5}MnO_3$ is $0.14\pm0.05\ e^-$, according to intermediate valence states of the form $Mn^{+3.43}$ and $Mn^{+3.57}$. Thus, this charge segregation is far from 1 electron, as for other half-doped manganites.[9,10]

According to our results, the observed charge disproportionation is not of electronic origin but determined by the structure. Thus, the so-called CO transition in Bi manganites derives from the structural transition due to a change in the lattice dynamics of the MnO_6 distortions as previously proposed for $LaMnO_3$ (Ref. 34). However, the extraordinarily high increase of the CO transition temperature in $Bi_{0.5}Sr_{0.5}MnO_3$ ($\sim$475 K) compared to $Nd_{0.5}Sr_{0.5}MnO_3$ ($\sim$150 K) strongly suggests that the fact that Bi^{3+} cations are heavier than La^{3+}, Pr^{3+} or Nd^{3+} should play an active role in the onset of this transition, favoring the condensation of phonon modes at higher temperatures.

At this point, it is also worth commenting on the intriguing anomaly at T_{CO} in the magnetic susceptibility,[18] while the sample remains paramagnetic. A similar effect was observed at the respective so-called CO and/or OO temperature in $Pr_{0.6}Ca_{0.4}MnO_3$ (Ref. 7) and $LaMnO_3$ (Ref. 35), respectively. When treated as a simple Curie-Weiss an increase in the effective moment is commonly found below T_{CO} in half-doped CO manganites. The ZP model[7] accounted for this unconventional paramagnetic behavior explaining the increase in the effective moment by the formation of Zener FM pairs as new paramagnetic units that they will order AF below T_N. Although our present RXS results support the occurrence of partial charge segregation (in contrast to Mn pairs having the same intermediate valence), the possibility of a FM coupling in the $Mn^{3-\delta}$-$Mn^{3+\delta}$ pair cannot be totally discarded. However, it is necessary to recognize that a satisfactory explanation for the susceptibility anomaly compatible with the CE single striped model is still lacking. Application of the Curie-Weiss law to the CE structure could be an oversimplification. An attempt to solve this controversy can be found in Ref. 36, applied to the CE compound $NaMn_7O_{12}$. Although the model in Ref. 36 cannot be satisfactorily applied to the susceptibility of our Bi compound, we cannot discard a change in the magnetic interaction between Mn ions responsible for the CE magnetic ordering crossing the transition.

VI. CONCLUSIONS

The low temperature phase (so-called CO phase) of a $Bi_{0.50}Sr_{0.50}MnO_3$ single crystal has been investigated by means of an RXS technique. Resonant effects were experimentally observed at energies close to the Mn K absorption edge for the weak superstructure (030) and (050) reflections and the forbidden $(0\ 5/2\ 0)$ and $(0\ 7/2\ 0)$ reflections. The energy, azimuthal, and polarization dependences of the scattered intensity for these reflections are well described using a checkerboard model with two nonequivalent Mn sites in terms of their local structure: one being isotropic (the three tensor components of the atomic scattering factor are equal) and the other anisotropic with two different tensor components, one perpendicular and the other parallel to the anisotropy axis. The information supplied by the resonant scattering at the $(4\ \frac{1}{2}\ 0)$ and $(3\ \frac{1}{2}\ 0)$ reflections has allowed us to conclude the existence of a transversal modulation of the Mn atoms. This lattice modulation agrees with a model of shared oxygen octahedra forming zigzag chains. Moreover, neither the bistriped arrangement[13,20] nor the ZP model[7] can account for the observed azimuthal and polarization dependences.

These experimental results suggest a structural transition at T_{CO} that stabilizes an ordering of the two Mn_1 and Mn_2 atoms in a checkerboard pattern. A semiempirical description of the energy dependence of the intensity of these reflections has allowed us to determine how different the two Mn atoms are regarding their chemical state and geometrical local structure. First, the charge difference between the two Mn atoms is about 0.14 electrons, far from the ideal Mn^{3+}/Mn^{4+} (1 electron) difference. Hence, the electron is not localized at the Mn site (MnO_6 cluster) and it is hard to define the Mn electronic configuration in terms of occupied and empty localized 3D (or 3D-like) orbitals. Second, the atomic anomalous scattering factor of the Mn_1 atom is anisotropic (the anisotropic energy splitting is about 1.5 eV). The symmetry of the anomalous scattering tensor is determined by the anisotropy of the local geometrical structure (distortion of the MnO_6 octahedron) so we can deduce that the Mn_1O_6 octahedron is tetragonal distorted with a well-defined elongation axis whereas the Mn_2O_6 octahedron is nearly regular (high point symmetry site). Then, the anisotropy of the projected electronic density of empty *p*-symmetry states at the Mn site, probed by dipolar RXS at the Mn *K* edge, is mainly sensitive to the details of the crystal and site symmetries. As it has been also recently shown in related oxides such as Fe, Co, and Mn ferrites,[37] the ATS (anisotropic tensor of susceptibility) reflections cannot be considered as a proof the OO of localized 3D (or 3D-like) states at the transition-metal site.

As our final conclusions, it seems that the checkerboard ordering of two distinct types of Mn octahedra is the ground state preferred for half-doped $A_{0.5}B_{0.5}MnO_3$ manganites, independent of the nature of the A and B atoms. Moreover, the charge disproportion markedly smaller than one electron[6,38,39] seems to be a rather common feature in high correlated transition-metal oxides. These conclusions invalidate the widely used ionic picture of CO and OO to interpret the appearance of these superstructure reflections in the low temperature phase, together with the jump in the resistivity at the transition.

ACKNOWLEDGMENTS

This work was financially supported by the Spanish CICyT Grant No. MAT02-01221 and the MEC (Grant No. MAT2003-07483-C02-02) projects. Financial support from Generalitat de Catalunya (Grants No. GRQ95-8029 and No. PICS2005-14) and DGA is also thanked. P.B. acknowledges financial support from MEC (Spain). We thank ESRF for granting beam time and C. Mazzoli (ESRF-ID20) for assistance with data collection and useful discussions.

*Author to whom correspondence should be addressed. Email address: jgr@unizar.es

[1] J. M. Tranquada, B. J. Sternlieb, J. D. Axe, Y. Nakamura, and S. Ishida, Nature (London) **375**, 561 (1995); H. A. Mook and F. Dogan, *ibid.* **401**, 145 (1999).

[2] Y. Moritomo, Y. Tomioka, A. Asamitsu, Y. Tokura, and Y. Matsui, Phys. Rev. B **51**, 3297 (1995); S. Mori, C. H. Chen, and S.-W. Cheong, Nature (London) **392**, 473 (1998).

[3] J. B. Goodenough, Phys. Rev. **100**, 564 (1955).

[4] P. G. Radaelli, D. E. Cox, M. Marezio, and S.-W. Cheong, Phys. Rev. B **55**, 3015 (1997).

[5] R. J. Goff and J. P. Attfield, Phys. Rev. B **70**, 140404(R) (2004).

[6] J. García and G. Subías, J. Phys.: Condens. Matter **16**, R145 (2004).

[7] A. Daoud-Aladine, J. Rodríguez-Carvajal, L. Pinsard-Gaudart, M. T. Fernández-Díaz, and A. Revcolevschi, Phys. Rev. Lett. **89**, 097205 (2002).

[8] J. García, M. C. Sánchez, J. Blasco, G. Subías, and M. G. Proietti, J. Phys.: Condens. Matter **13**, 3243 (2001).

[9] S. Grenier, J. P. Hill, D. Gibbs, K. J. Thomas, M. V. Zimmerman, C. S. Nelson, V. Kiryukhin, Y. Tohura, Y. Tomioka, D. Casa, T. Gog, and C. Venkataraman, Phys. Rev. B **69**, 134419 (2004).

[10] J. Herrero-Martín, J. García, G. Subías, J. Blasco, and M. C. Sánchez, Phys. Rev. B **70**, 024408 (2004).

[11] V. A. Bokov, N. A. Grigoryan, and H. F. Bryzhina, Phys. Status Solidi **20**, 745 (1967).

[12] J. L. García-Muñoz, C. Frontera, M. A. G. Aranda, A. Llobet, and C. Ritter, Phys. Rev. B **63**, 064415 (2001).

[13] M. Hervieu, A. Maignan, C. Martin, N. Nguyen, and B. Raveau, Chem. Mater. **13**, 1356 (2001).

[14] C. Frontera, J. L. García-Muñoz, M. A. G. Aranda, M. Hervieu, C. Ritter, Ll. Mañosa, X. G. Capdevila, and A. Calleja, Phys. Rev. B **68**, 134408 (2003).

[15] R. D. Shannon, Acta Crystallogr., Sect. A: Cryst. Phys., Diffr., Theor. Gen. Crystallogr. **32**, 751 (1976).

[16] H. Chiba, T. Atou, and Y. Syono, J. Solid State Chem. **132**, 139 (1997).

[17] C. Frontera, J. L. García-Muñoz, A. Llobet, M. A. G. Aranda, C. Ritter, M. Respaud, and J. Vanacken, J. Phys.: Condens. Matter **13**, 1071 (2001).

[18] J. Hejtmánek, K. Knízek, Z. Jirák, M. Hervieu, C. Martin, M. Nevriva, and P. Beran, J. Appl. Phys. **93**(10), 7370 (2003).

[19] J. L. García-Muñoz, C. Frontera, M. A. G. Aranda, C. Ritter, A. Llobet, M. Respaud, M. Goiran, H. Rakoto, O. Masson, J. Vanacken, and J. M. Broto, J. Solid State Chem. **171**, 84 (2003).

[20] M. Hervieu, S. Malo, O. Perez, P. Beran, C. Martin, and B. Raveau, Chem. Mater. **15**, 523 (2003).

[21] A. Stunault, C. Vettier, F. de Bergevin, N. Bernhoeft, V. Férnandez, S. Langridge, E. Lidström, J. E. Lorenzo-Díaz, D. Wermeille, L. Chabert, and R. Chagnon, J. Synchrotron Radiat. **5**, 1010 (1998).

[22] G. Materlik, C. J. Sparks, and H. Fisher, *Resonant Anomalous X-ray Scattering: Theory and Applications* (Elsevier Science B. V., North-Holland, 1994).

[23] H. Stragier, J. O. Cross, J. J. Rehr, L. B. Sorensen, C. E. Bouldin, and J. C. Woicik, Phys. Rev. Lett. **69**, 3064 (1992); J. J. Pickering, M. Sansone, J. Marsch, and S. N. George, J. Am. Chem. Soc. **115**(14), 6302 (1993).

[24] M. V. Zimmermann, C. S. Nelson, J. P. Hill, D. Gibbs, M. Blume, D. Casa, B. Keimer, Y. Murakami, C.-C. Kao, C. Venkataraman,

T. Gog, Y. Tomioka, and Y. Tokura, Phys. Rev. B **64**, 195133 (2001).

[25] C. H. Chen, S. Mori, and S.-W. Cheong, Phys. Rev. Lett. **83**, 4792 (1999); R. Kajimoto, H. Yoshizawa, Y. Tomioka, and Y. Tokura, Phys. Rev. B **63**, 212407 (2001).

[26] D. H. Templeton and L. K. Templeton, Acta Crystallogr. **36**, 237 (1980); V. E. Dmitrienko, Acta Crystallogr., Sect. A: Found. Crystallogr. **39**, 29 (1983); **40**, 89 (1984).

[27] Y. Wakabayashi, Y. Murakami, I. Koyama, T. Kimura, Y. Tokura, Y. Moritomo, Y. Endoh, and K. Hirota, J. Phys. Soc. Jpn. **72**, 618 (2003).

[28] C. Brouder, J. Phys.: Condens. Matter **2**, 701 (1990).

[29] A. Bianconi, in *X-ray Absorption: Principles, Applications, Techniques of EXAFS, SEXAFS and XANES*, edited by D. C. Koningsberger and R. Prins (Wiley, New York, 1988).

[30] R. W. James, *The Optical Principles of the Diffraction of X-rays* (G. Bell and Sons, London, 1948).

[31] D. T. Cromer and D. Liberman, J. Chem. Phys. **53**, 1891 (1970).

[32] M. Benfatto, Y. Joly, and C. R. Natoli, Phys. Rev. Lett. **83**, 636 (1999).

[33] G. Subías, J. García, M. G. Proietti, and J. Blasco, Phys. Rev. B **56**, 8183 (1997).

[34] M. C. Sánchez, G. Subías, J. García, and J. Blasco, Phys. Rev. Lett. **90**, 045503 (2003).

[35] J. S. Zhou and J. B. Goodenough, Phys. Rev. B **60**, R15002 (1999).

[36] F. Bolzoni, A. Prodi, A. Gauzzi, E. Gilioli, F. Licci, and M. Marezio, Phys. Rev. B **71**, 052404 (2005).

[37] G. Subías, J. García, M. G. Proietti, J. Blasco, H. Renevier, J. L. Hodeau, and M. C. Sánchez, Phys. Rev. B **70**, 155105 (2004).

[38] G. Subías, J. García, J. Blasco, M. G. Proietti, H. Renevier, and M. C. Sánchez, Phys. Rev. Lett. **93**, 156408 (2004).

[39] J. A. Alonso, J. L. García-Muñoz, M. T. Fernández-Díaz, M. A. G. Aranda, M. J. Martinez-Lope, and M. T. Casais, Phys. Rev. Lett. **82**, 3871 (1999).